Chinese Chemical Letters 33 (2022) 537–540

Contents lists available at ScienceDirect

Chinese Chemical Letters

journal homepage: www.elsevier.com/locate/cclet

Near UV luminescent $Cs_2NaBi_{0.75}Sb_{0.25}Cl_6$ perovskite colloidal nanocrystals with high stability

Huixian Yang[a], Yanmei Guo[a], Guoning Liu[a,*], Ruowei Song[a], Jinxi Chen[a], Yongbing Lou[a,*], Yixin Zhao[b,*]

[a] School of Chemistry and Chemical Engineering, Jiangsu Key Laboratory for Science and Application of Molecular Ferroelectrics, Jiangsu Engineering Laboratory of Smart Carbon-Rich Materials and Devices, Southeast University, Nanjing 211189, China
[b] School of Environmental Science and Engineering, Shanghai Jiao Tong University, Shanghai 200240, China

ARTICLE INFO

Article history:
Received 2 April 2021
Revised 14 May 2021
Accepted 31 May 2021
Available online 20 June 2021

Keywords:
Perovskite nanocrystals
Ligand-assisted reprecipitation
Stability
$Cs_2NaBiCl_6$
$Cs_2NaBi_{0.75}Sb_{0.25}Cl_6$

ABSTRACT

Near UV highly luminescent colloidal $Cs_2NaBiCl_6$ nanocrystals (NCs) were synthesized by a simple low-cost ligand-assisted reprecipitation method. In our strategy, metal chloride precursors were added to the mixture of anti-solvent and ligand at room-temperature. The obtained $Cs_2NaBiCl_6$ NCs exhibited a bright blue emission with significantly improved photoluminescence quantum yield (PLQY) of 39.05%. The optical properties and stability were greatly enhanced by doping Sb where $Cs_2NaBi_{0.75}Sb_{0.25}Cl_6$ showed a high PLQY of 46.57%, and both the powder and the colloidal solution exhibited superior stability.

In the past decade, colloidal lead halide perovskite nanocrystals (NCs) have aroused widespread interests due to their excellent photoelectric properties and potential application in light-emitting devices (LEDs) [1-3]. However, the instability in air and aqueous medium as well as lead toxicity issues hindered their employments [4-6]. Therefore, finding a lead-free alternative with optical properties comparable to the compounds has become the focus of current research. One of the most effective strategies was to replace the lead with divalent cations such as Sn^{2+} or Ge^{2+}. Unfortunately, the related materials exhibited poor crystal structural stability which was attributed to the facile oxidation to Sn^{4+} or Ge^{4+} in air, bringing about defects to cause photoluminescence (PL) quenching [7]. Another popular alternative approach was to substitute the two Pb^{2+} ions with a pair of singly-charged and triply-charged metal ions to form two kinds of octahedron, which led to a $A_2M'M''X_6$ (A: monovalent cation, X: halogen anion, M′: + 1 cation, M″: + 3 cation) three dimensional (3D) double perovskite structure [8,9]. The lead-free double perovskite NCs were expected to be excellent candidate in photoelectric field because of their 3D structure, eco-friendly and stability [10].

Currently, different colloidal double perovskite NCs such as Cs_2AgBiX_6, Cs_2AgInX_6, Cs_2AgSbX_6, $Cs_2NaBiCl_6$ and $Cs_2NaInCl_6$ have been synthesized *via* various methods. One of the mostly used approaches was hot-injection in which one precursor was injected into another solution under the condition of N_2 environment and high temperature. Another strategy was the ligand-assisted reprecipitation (LARP) route, where ions in the polar solvent was immediately destabilized by adding into an anti-solvent, thereby causing a nucleation explosion [11]. However, low photoluminescence quantum yield (PLQY) and ambient instability still remained to be the obstacles of wide application for double perovskite NCs, which were attributed to the indirect band gaps [12,13]. For the purpose of improving the PLQYs of these NCs, different doping strategies have been explored such as incorporating Cu^{2+}, Mn^{2+}, and lanthanide ions [14,15]. Alternative processes, mainly aimed at engineering the band gap of double perovskites, involved the synthesis of quinary compounds by employing a combination of B^+ or B^{3+} ions. Previous reports showed that impurity ions (*e.g.*, Mn^{2+}, Yb^{3+}/Er^{3+} and Bi^{3+} ions) could be successfully introduced into $Cs_2AgInCl_6$ NCs and remarkable PL improvements were obtained [16,17]. PLQY of 36.6% for Bi-alloyed $Cs_2AgInCl_6$ NCs was observed which was comparable to traditional lead perovskite NCs [18,19]. The PLQY of Na and Bi alloyed $Cs_2AgInCl_6$ NCs was as high as 64%, and the emission color varies with its composition and size [20,21]. In addition to Ag-based perovskite NCs, $Cs_2NaBiCl_6$ NCs were mainly prepared by hot-injection with very low PLQY. Besides, $Cs_2NaBiCl_6$ NCs showed high flexibility for different ion doping to enhance its photoelectric properties. Recently, Mn-doped

* Corresponding authors.
E-mail addresses: liuguoning234232@163.com (G. Liu), lou@seu.edu.cn (Y. Lou), yixin.zhao@sjtu.edu.cn (Y. Zhao).

https://doi.org/10.1016/j.cclet.2021.05.071
1001-8417/

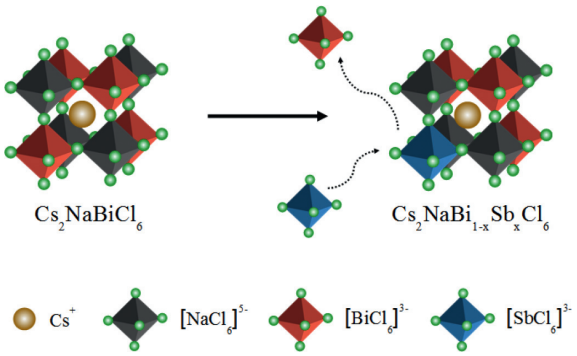

Scheme 1. Schematic presentation of the crystal structures of the $Cs_2NaBiCl_6$ material and their $Cs_2NaBi_{1-x}Sb_xCl_6$ mixed Bi/Sb cationic analogues.

$Cs_2NaBiCl_6$ NCs with an improved PLQY of 15% were reported [22-24]. As investigated by Yao *et al*., Ag-doped $Cs_2NaBiCl_6$ NCs exhibited a high PLQY of 20%, which has attracted great attention on the doped lead-free $Cs_2NaBiCl_6$ NCs [25].

Sb^{3+}, with an electronic structure of ns^2, is an important metal ion for double perovskites owing to its close energy levels to other B^{3+} ions and unique luminescence characteristics [26]. Currently, Sb-doping strategy was successfully applied in Cs_2SnCl_6, $Cs_2AgInCl_6$ and $Cs_2NaInCl_6$. For instance, Sb^{3+} alloyed $Cs_2NaInCl_6$ microcrystals showed PLQYs of 78.9% and 79% respectively. Also, by the incorporation of Sb^{3+}, an excellent PLQY (~37%) of the vacancy-ordered double perovskite Cs_2SnCl_6 was obtained [27]. Besides, through a gradual substitution of Sb with In in a solid solution experiment of $Cs_2AgSb_{1-x}In_xCl_6$, the bandgap transformed from direct to indirect [28]. In this paper, $Cs_2NaBiCl_6$ NCs prepared by a simple LARP approach showed bright blue photoluminescence emission with a record high PLQY of 39.05%. After incorporating Sb, the PLQY increased to 46.57%, that is, for the $Cs_2NaBi_{0.75}Sb_{0.25}Cl_6$ stoichiometry. Moreover, the powder and the solution of $Cs_2NaBi_{0.75}Sb_{0.25}Cl_6$ exhibited superior stability under air which would make it promising for commercial application.

The crystal structures of $Cs_2NaBi_{1-x}Sb_xCl_6$ (x = 0, 0.25, 0.5, 0.75, 1) NCs were shown in Scheme 1. The $Cs_2NaBiCl_6$ crystal adopted a typical 3D framework of double perovskite with Cs atoms in the center and octahedrons consisting of corner-sharing $[NaCl_6]^{5-}$ and $[BiCl_6]^{3-}$ while Sb^{3+} ions were incorporated into $Cs_2NaBiCl_6$ NCs and occupied Bi^{3+} sites to form $Cs_2NaBi_{1-x}Sb_xCl_6$ crystals [29]. The synthesis of $Cs_2NaBi_{1-x}Sb_xCl_6$ (x = 0, 0.25, 0.5, 0.75, 1) NCs were carried out by a simple low-cost LARP route as well as by tuning the molar ratios of $BiCl_3$ and $SbCl_3$ in the precursor. Details were discussed in Supporting information. Also, the influence of different amounts of oleic acid (OA) and precursors were explored for better optical properties, where 100 μL precursor solution and 3% OA were found to be the optimal condition for the reaction (Figs. S1a-d in Supporting information). As shown in Fig. 1a, the X-ray diffraction (XRD) patterns of $Cs_2NaBiCl_6$ and $Cs_2NaBi_{0.75}Sb_{0.25}Cl_6$ NCs were consistent with $Cs_2NaBiCl_6$ (PDF#77–1831), indicating that the NCs were pure and highly crystalline in the *Fm 3 m* space group. The ordered arrangements of Na^+ and Bi^{3+} were evidenced by the strong intensity of the (1 1 1) peak. The (4 0 0) peak shifted toward higher angles as the amount of Sb^{3+} increased, which was attributed to the lattice contraction (Fig. S2 in Supporting information) [26]. Notably, the intensity of (1 1 1) and (3 1 1) peaks gradually decreased with higher Sb^{3+} ratios (x > 0.25), while an impure phase $Cs_3Sb_2Cl_9$ appeared in Sb-rich condition (Fig. 1a) [30]. The low alloying level of Sb was probably due to the larger radius difference between Na^+ (0.102 nm) and Sb^{3+} (0.076 nm) comparing to that of Na^+ (0.102 nm) and Bi^{3+} (0.103 nm). In order to reveal the accurate stoichiometric ratios of the metal ions (Bi^{3+} and Sb^{3+}) in $Cs_2NaBi_{0.75}Sb_{0.25}Cl_6$, the inductively coupled plasma-optical emission spectrometry (ICP-OES) measurement was conducted. The feeding molar amount of (Bi^{3+} and Sb^{3+}) was equal to that of Na^+ so that the calculated molar ratios of Bi/Na and Sb/Na could represent the actual values of $1 - x$ and x (Table S1 in Supporting information). The results indicated that the actual amount of Sb^{3+} was much lower than the chemical formula composition, which was common in other doped double perovskites [26,12]. As shown in transmission electron microscopy (TEM) images, the $Cs_2NaBiCl_6$ and $Cs_2NaBi_{0.75}Sb_{0.25}Cl_6$ NCs were spherical-shaped (Figs. 1c and d) with average sizes of 10.03 ± 0.34 nm and 7.01 ± 0.16 nm, respectively (Figs. 1e and f). From the high-resolution TEM (HRTEM), it could be observed that the lattice distances of the NCs were measured to be 0.33 nm, corresponding to the (3 1 1) plane (insets in Figs. 1c and d). The analysis above revealed that the alloy of Sb^{3+} would not produce additional vacancies and interstitial defects. Therefore, no additional surface trapping states would occur after doping and the intrinsic optical properties were significantly enhanced [31].

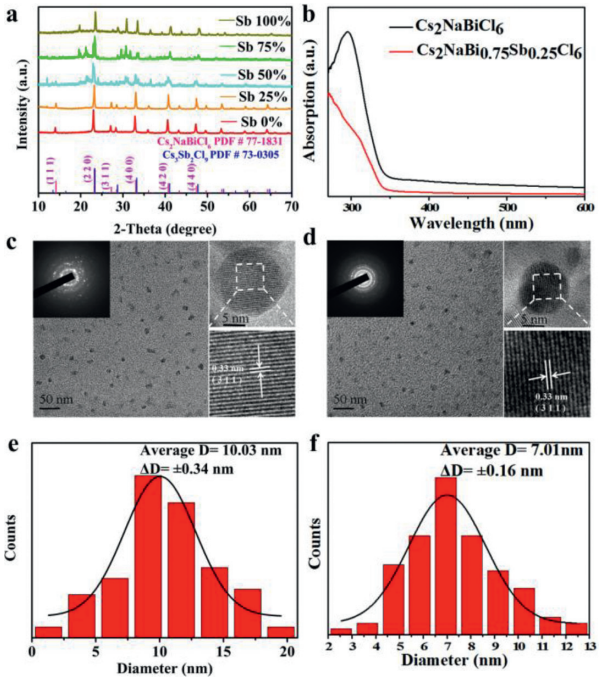

Fig. 1. (a) XRD patterns of $Cs_2NaBi_{1-x}Sb_xCl_6$ (x = 0, 0.25, 0.5, 0.75, 1). (b) Steady-state absorption spectra of $Cs_2NaBiCl_6$ and $Cs_2NaBi_{0.75}Sb_{0.25}Cl_6$. (c, d) Low-resolution TEM images of $Cs_2NaBiCl_6$ and $Cs_2NaBi_{0.75}Sb_{0.25}Cl_6$ NCs (insets: electron diffraction patterns and associated HRTEM images). (e, f) The size distributions of $Cs_2NaBiCl_6$ and $Cs_2NaBi_{0.75}Sb_{0.25}Cl_6$ NCs.

In order to further clarify the presence of Sb^{3+}, the X-ray photoelectron spectroscopy (XPS) technique was conducted. The full spectra revealed that Cs, Na, Bi, Cl existed in both $Cs_2NaBiCl_6$ and $Cs_2NaBi_{0.75}Sb_{0.25}Cl_6$ NCs (Fig. S3 in Supporting information). As shown in Fig. S3d, two peaks of Sb 3d appearing at 539 eV and 531 eV in $Cs_2NaBi_{0.75}Sb_{0.25}Cl_6$ sample confirmed the successful incorporation of Sb^{3+} ions in $Cs_2NaBiCl_6$ NCs. Furthermore, compared the high-resolution XPS spectra of Bi 4f and Na 1s of $Cs_2NaBi_{0.75}Sb_{0.25}Cl_6$ and $Cs_2NaBiCl_6$ NCs (Fig. S4 in Supporting information), the binding energy of Bi 4f shifted slightly to lower energy while Na 1s has little variations. The slight shift could be attributed to the lattice contraction caused by the introduction of Sb^{3+} ions, probing the above speculation that Sb^{3+} ions occupied Bi^{3+} sites instead of Na^+sites [32].

Next, the steady-state optical properties of $Cs_2NaBiCl_6$ and $Cs_2NaBi_{0.75}Sb_{0.25}Cl_6$ NCs were investigated. Bright blue-violet

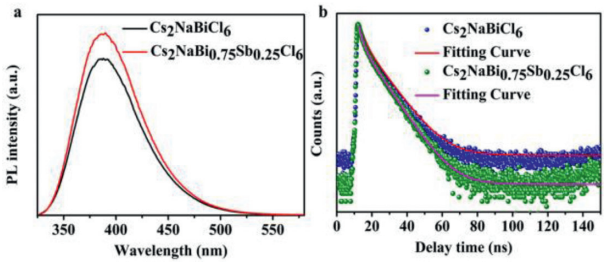

Fig. 2. (a) PL spectra of $Cs_2NaBiCl_6$ and $Cs_2NaBi_{0.75}Sb_{0.25}Cl_6$ NCs. (b) Time-resolved PL traces of $Cs_2NaBiCl_6$ and $Cs_2NaBi_{0.75}Sb_{0.25}Cl_6$ NCs measured with TCSPC.

emission could be seen under UV lamp (Fig. S5 in Supporting information). From the absorption spectra, it was observed that a prominent absorption peak appeared at 295 nm for $Cs_2NaBiCl_6$ while a broad peak at 312 nm was shown for $Cs_2NaBi_{0.75}Sb_{0.25}Cl_6$ NCs (Fig. 1b). The 295 nm absorption peak could be assigned to $^1S_0 \rightarrow {}^3P_2$ forbidden transition whereas the 312 nm peak was associated with $^1S_0 \rightarrow {}^3P_1$ partially allowed transition of the localized $[BiCl_6]^{3-}$ octahedron in colloidal solution [33]. The band gap, calculated from the corresponding Tauc plot, fell at 3.04 eV and 2.92 eV which illustrated a red-shift trend (Fig. S6 in Supporting information). According to the previous research, the valence band was shifted up by the incorporation of Sb^{3+} 5s orbitals while the 5p orbitals of Sb^{3+} caused a lower conduction band, resulting in a narrower band gap [31].

To look deep into the luminescence features of $Cs_2NaBiCl_6$ and $Cs_2NaBi_{0.75}Sb_{0.25}Cl_6$ NCs, PL spectra and PLQYs of these NCs were studied. The highest emission intensity was observed for 25% Sb-doped $Cs_2NaBiCl_6$ NCs. Meanwhile, the slight decrease in luminescence intensity was clearly visible in PL spectrum for the higher Sb^{3+} contents, which was due to the concentration quenching and the presence of by-product $Cs_3Sb_2Cl_9$. (Fig. S7 in Supporting information) [33]. In contrary to the weak emission with a low PLQY of $Cs_2NaBiCl_6$ NCs in published literature, the pristine $Cs_2NaBiCl_6$ prepared by LARP route exhibited a PLQY up to 39.05% (Fig. S8 in Supporting information). By using hot-injection method, inhomogeneous morphologies and impurity CsCl were found under different temperature which probably led to the low PLQY. Thus, the LARP approach used in this work effectively avoided such shortcomings and the ligand (OA) passivated the surface defects of the NCs, resulting in an improved PLQY [25]. Interestingly, the PL peak position of $Cs_2NaBiCl_6$ and $Cs_2NaBi_{0.75}Sb_{0.25}Cl_6$ showed no variation (Fig. 2a), which indicated that the PL transition was derived from the radiative recombination of the internal energy states instead of the band-edge electrons/holes recombination [31]. It was proposed that the self-trapped excitons (STEs) played an important role in the emission process. The observable PL in $Cs_2NaBiCl_6$ was attributed to the dark state STEs [31]. After trace Sb^{3+} doping, the emission intensity was greatly improved while maintaining the same peak position at 388 nm, which illustrated that the dark STEs in $Cs_2NaBiCl_6$ transformed to bright STEs in $Cs_2NaBi_{0.75}Sb_{0.25}Cl_6$ [12]. The transition from dark state to bright state was probably related to two aspects. Firstly, the parity-forbidden transition could be broken by the interaction of $[SbCl_6]^{3-}$ and $[BiCl_6]^{3-}$, resulting in effective PL emission. Secondly, reduced lattice vibrations could increase radiative recombination pathway [12]. To prove the smaller lattice vibrations caused by Sb^{3+} doping, Raman spectra was investigated (Fig. S9 in Supporting information). It was obvious that the peak position of $Cs_2NaBiCl_6$ and $Cs_2NaBi_{0.75}Sb_{0.25}Cl_6$ remained the same, but the vibration intensity decreased after alloying Sb [12]. More importantly, the PLQY value of $Cs_2NaBi_{0.75}Sb_{0.25}Cl_6$ NCs was measured to be 46.57% (Fig. S8), suggesting a significant improvement compared to other ion alloyed $Cs_2NaBiCl_6$ NCs (Table S2 in Supporting information). For the purpose of better understanding the mechanism, the wavelength-dependent PL emission spectrum and PL excitation (PLE) spectrum of $Cs_2NaBi_{0.75}Sb_{0.25}Cl_6$ were carried out. The PL curves were almost the same at different excited wavelength which proved that the emission was not aroused from permanent defects (Fig. S10a in Supporting information) [12]. The almost same PLE profile verified the same excited state origin of these emission bands (Fig. S10b in Supporting information) [31]. As shown in Scheme S1 (Supporting information), the emission energy of STE could be calculated by the formula: $E_{STE} = E_g - E_b - E_{st} - E_d$ where E_g represents the band gap, E_b represents the binding energy of free exciton, E_{st} represents the self-trapping energy, and E_d represents the lattice deformation energy [34]. Based on the strong exciton-phonon coupling existed in pure $Cs_2NaBiCl_6$ and $Cs_2NaSbCl_6$ [26], $Cs_2NaBi_{0.75}Sb_{0.25}Cl_6$ promoted the formation of STEs and produced small E_{st} and E_d. Therefore, the values of E_{STE} and E_g was very close which could lead to the strong blue emission [31].

In order to shed more light on the recombination dynamics of $Cs_2NaBiCl_6$ and $Cs_2NaBi_{0.75}Sb_{0.25}Cl_6$ NCs and clarify the implication of Sb, time-resolved PL (TR-PL) measurements using time-correlated single photon counting (TCSPC) was carried out. The two decay curves could be fitted well by a biexponential function (Fig. 2b). For $Cs_2NaBiCl_6$, a fast decay component (short lifetime τ_1) assigned to charge carrier trapping processes was about 2.5 ns and a slow decay component (long lifetime τ_2) associated with the band-to-band radiative recombination was 9.8 ns. For $Cs_2NaBi_{0.75}Sb_{0.25}Cl_6$, a long-lived lifetime of 8.7 ns and a short-lived lifetime of 1.9 ns were obtained (Table S3 in Supporting information). It was well-known that the ground state of Sb^{3+} was represented by the $^1S_0$ atomic term, and four energy levels of $^1P_1$, $^3P_0$, $^3P_1$ and $^3P_2$ constituted the excited state (sp). The $^1S_0 - {}^1P_1$ transition was allowed, and the $^1S_0 - {}^3P_1$ transition was partially-allowed because of the spin-orbit coupling, while the $^1S_0 - {}^3P_2$ and $^1S_0 - {}^3P_0$ transitions were completely prohibited at the electric dipole transition level [35]. Upon the theory and research of Reisfeld *et al.*, it was reasonable to speculate that there could exist two recombination routes. One was the excited state of $^3P_0 \rightarrow {}^1S_0$ recombination in Sb^{3+} with a faster decay rate and the other was the excited state of $^3P_1 \rightarrow {}^1S_0$ with a slower decay rate [35]. It meant that the incorporation of Sb^{3+} increased the possibility of radiation recombination by breaking the local symmetry so that the initial parity-forbidden transition could occur, which led to the improvement of PLQY [21]. Besides, both the percentages of τ_1 and τ_2 of $Cs_2NaBiCl_6$ were 50% while the percentages of τ_1 and τ_2 of $Cs_2NaBi_{0.75}Sb_{0.25}Cl_6$ were 49% and 51%. The similar percentages of two NCs represented the same emission mechanism which is consistent with the inference that Sb alloying caused STEs to change from dark state to bright state.

The stability of perovskite NCs was also directly relevant to the industrial applications. To evaluate the air stability of $Cs_2NaBiCl_6$ and $Cs_2NaBi_{0.75}Sb_{0.25}Cl_6$ NCs solutions, the PL evolution was measured with different storage time in ambient atmosphere. As illustrated in Fig. 3a, the PL intensity in first few days of two solutions increased slightly which was assigned to the elimination of dangling bonds [36]. With the increasing time placed in air, the PL intensity gradually declined owing to the formation of surface defects after air exposure [36]. It was worth noting that the $Cs_2NaBi_{0.75}Sb_{0.25}Cl_6$ solution retained 91% of original photoluminescence after 40 days while $Cs_2NaBiCl_6$ solution retained only 83% of original photoluminescence after 26 days (Fig. 3a). Furthermore, the powder of $Cs_2NaBi_{0.75}Sb_{0.25}Cl_6$ NCs exhibited better stability in air, maintaining the XRD pattern even after 5 months (Fig. 3b), where impurity appeared in the XRD pattern of undoped $Cs_2NaBiCl_6$ sample (Fig. 3c). The higher air stability of $Cs_2NaBi_{0.75}Sb_{0.25}Cl_6$ NCs compared to undoped NCs was at-

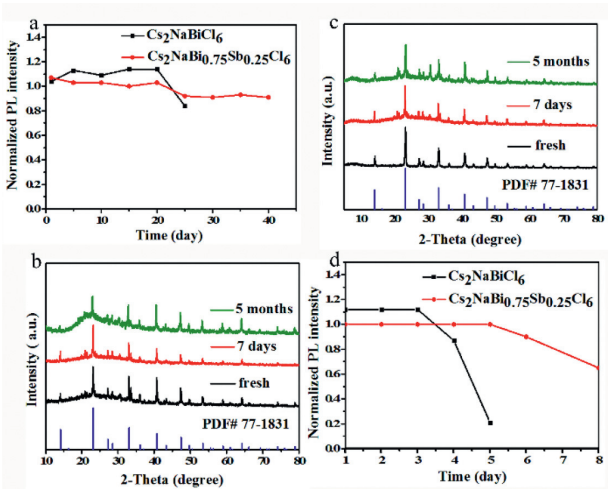

Fig. 3. (a) The percentages of PL intensity of $Cs_2NaBiCl_6$ (3.4 mg/mL) and $Cs_2NaBi_{0.75}Sb_{0.25}Cl_6$ (2.3 mg/mL) solutions at different times when exposed to air. The XRD patterns of (b) $Cs_2NaBi_{0.75}Sb_{0.25}Cl_6$ powder and (c) $Cs_2NaBiCl_6$ powder after 7 days and 5 months being placed in the air. (d) The percentages of PL intensity at different times when 3% water were added to 5 mL supernatant of two NCs.

tributed to the reduction of volume defects which resulted in the improvement of short-range order of the $Cs_2NaBi_{0.75}Sb_{0.25}Cl_6$ NCs [12]. Moreover, the water-stability of the $Cs_2NaBiCl_6$ and $Cs_2NaBi_{0.75}Sb_{0.25}Cl_6$ colloidal solution were investigated by adding 3% deionized water. It was observed that $Cs_2NaBi_{0.75}Sb_{0.25}Cl_6$ remained 68% of initial intensity after 8 days while the intensity of $Cs_2NaBiCl_6$ was dropped to merely 20% after 5 days (Fig. 3d). The better water-stability was probably due to the formation of SbOCl on the surface. The XPS peaks located at 540.0 eV and 532.9 eV were associated with Sb^{3+} $3d_{3/2}$ and $3d_{5/2}$. An additional peak of Sb-O at 531.7 eV appeared (Fig. S11a in Supporting information), which was attributed to the presence of Sb-O on the crystal surface due to the hydrolysis of antimony chloride. Besides, the XRD patterns of $Cs_2NaBi_{0.75}Sb_{0.25}Cl_6$ before and after adding water were investigated (Fig. S11b in Supporting information), where SbOCl phase was identified in $Cs_2NaBi_{0.75}Sb_{0.25}Cl_6$ after adding 3% water [27]. All the results demonstrated the superior stability of $Cs_2NaBi_{0.75}Sb_{0.25}Cl_6$ comparing to various ion doping strategies used for $Cs_2NaBiCl_6$ NCs in the literatures (Table S4 in Supporting information). The excellent air-stability of $Cs_2NaBi_{0.75}Sb_{0.25}Cl_6$ NCs laid a solid foundation of its wide application and the research results provided a new example for the future study of Sb-based double perovskite.

In summary, $Cs_2NaBiCl_6$ NCs were fabricated *via* a room-temperature LARP approach with a high PLQY of 39.05%. The strategy was extended to the synthesis of $Cs_2NaBi_{0.75}Sb_{0.25}Cl_6$ NCs, which showed a strong blue photoluminescence with an improved PLQY of 46.57%. Additionally, the powder and the solution of $Cs_2NaBi_{0.75}Sb_{0.25}Cl_6$ NCs exhibited superior stability in ambient environment. The excellent optical performance and outstanding stability of $Cs_2NaBi_{0.75}Sb_{0.25}Cl_6$ perovskite NCs prepared by this simple route would expand its potential application for optoelectronic devices.

Declaration of competing interest

The authors declare no competing financial interest.

Acknowledgments

This work was sponsored by the National Natural Science Foundation of China (Nos. 21475021, 21427807 and 21777096), the Priority Academic Program Development of Jiangsu Higher Education Institutions.

Supplementary materials

Supplementary material associated with this article can be found, in the online version, at doi:10.1016/j.cclet.2021.05.071.

References

[1] Z. Xiao, Z. Song, Y. Yan, Adv. Mater. 31 (2019) 1803792.
[2] L. Chu, W. Ahmad, W. Liu, et al., Nano-Micro Lett. 11 (2019) 16.
[3] X. Liu, J. Gao, G. Zhou, et al., J. Mol. Liq. 299 (2020) 112199.
[4] S. Liu, B. Yang, J. Chen, et al., Angew. Chem. Int. Ed. 132 (2020) 22109–22113.
[5] Z. Tan, Y. Chu, J. Chen, et al., Adv. Mater. 32 (2020) 2002443.
[6] G. Qiao, L. Liu, X. Hao, et al., Chem. Eng. J. 382 (2020) 122907.
[7] S. Li, Z. Shi, F. Zhang, et al., ACS Appl. Mater. Interfaces 12 (2020) 46330–46339.
[8] M. Keshavarz, E. Debroye, M. Ottesen, et al., Adv. Mater. 32 (2020) 2001878.
[9] Q. Fan, G.V. Biesold-McGee, J. Ma, et al., Angew. Chem. Int. Ed. 59 (2020) 1030–1046.
[10] D. Zhu, J. Zito, V. Pinchetti, et al., ACS Energy Lett. 5 (2020) 1840–1847.
[11] K. Lv, S. Qi, G. Liu, et al., Chem. Commun. 55 (2019) 14741–14744.
[12] P. Han, X. Mao, S. Yang, et al., Angew. Chem. Int. Ed. 58 (2019) 17231–17235.
[13] Z. Xia, Y. Liu, A. Nag, L. Manna, Angew. Chem. Int. Ed. 133 (2020) 2–14.
[14] Y. Liu, X. Rong, M. Li, et al., Angew. Chem. Int. Ed. 59 (2020) 11634–11640.
[15] F. Locardi, M. Cirignano, D. Baranov, et al., J. Am. Chem. Soc. 140 (2018) 12989–12995.
[16] H. Arfin, J. Kaur, T. Sheikh, S. Chakraborty, A. Nag, Angew. Chem. Int. Ed. 59 (2020) 11307–11311.
[17] N. Chen, T. Cai, W. Li, et al., ACS Appl. Mater. Interfaces 11 (2019) 16855–16863.
[18] D. Manna, J. Kangsabanik, T.K. Das, et al., J. Phys. Chem. Lett. 11 (2020) 2113–2120.
[19] B. Yang, X. Mao, F. Hong, et al., J. Am. Chem. Soc. 140 (2018) 17001–17006.
[20] F. Locardi, E. Sartori, J. Buha, et al., ACS Energy Lett. 4 (2019) 1976–1982.
[21] R.S. Lamba, P. Basera, S. Bhattacharya, S. Sapra, J. Phys. Chem. Lett. 10 (2019) 5173–5181.
[22] W. Lee, D. Choi, S. Kim, Chem. Mater. 2 (2020) 6864–6874.
[23] X. Liu, X. Xu, B. Li, et al., Small 16 (2020) 2002547.
[24] J.D. Majher, M.B. Gray, T.A. Strom, P.M. Woodward, Chem. Mater. 31 (2019) 1738–1744.
[25] M.M. Yao, L. Wang, J.S. Yao, et al., Adv. Optical Mater. 8 (2020) 1901919.
[26] S. Wu, W. Li, J. Hu, P. Gao, J. Mater. Chem. C 8 (2020) 13603–13611.
[27] J. Li, Z. Tan, M. Hu, et al., Front. Optoelec. 12 (2019) 352–364.
[28] S. Khalfin, Y. Bekenstein, Nanoscale 11 (2019) 8665–8679.
[29] A. Karmakar, G.M. Bernard, A. Meldrum, A.O. Oliynyk, V.K. Michaelis, J. Am. Chem. Soc. 142 (2020) 10780–10793.
[30] B. Yang, F. Hong, J. Chen, et al., Angew. Chem. Int. Ed. 58 (2019) 2278–2283.
[31] R. Zeng, L. Zhang, Y. Xue, et al., J. Phys. Chem. Lett. 11 (2020) 2053–2061.
[32] M. Shi, G. Li, W. Tian, et al., R. Li, C. Li, Adv. Mater. 32 (2020) 2002137.
[33] M.B. Gray, S. Hariyani, T.A. Strom, et al., J. Mater. Chem. C 8 (2020) 6797–6803.
[34] J. Luo, X. Wang, S. Li, et al., Nature 563 (2018) 541–545.
[35] A. Noculak, V. Morad, K.M. McCall, et al., Chem. Mater. 32 (2020) 5118–5124.
[36] P. Yang, G. Liu, B. Liu, et al., Chem. Commun. 54 (2018) 11638–11641.